Research Article

Read F. Alserihi, Mohammed Razeeth Shait Mohammed, Mohammed Kaleem, Mohammad Imran Khan, Mario Sechi, Vanna Sanna, Torki A. Zughaibi, Adel M. Abuzenadah, and Shams Tabrez*

Development of (−)-epigallocatechin-3-gallate-loaded folate receptor-targeted nanoparticles for prostate cancer treatment

https://doi.org/10.1515/ntrev-2022-0013
received October 4, 2021; accepted December 6, 2021

Abstract: In continuation of our previous studies, we developed polymeric epigallocatechin 3-gallate (EGCG)-loaded nanoparticles (NPs) coupled with folic acid (FA), able to dually bind the human folate receptor alpha (FOLR1), and prostate-specific membrane antigen ($PSMA^+$) in prostate cancer (PCa) model. After a preliminary computational molecular recognition of NP′ ligand binding on the FOLR1 active site, we synthesized the biocompatible block-copolymer PLGA–PEG–FA to prepare EGCG-targeted NPs (EGCG-T-NPs). The obtained NPs were characterized by various analytical techniques, and anticancer efficacy was determined by different sets of experiments in a 3D culture of PCa using PC3 and 22Rv1 cell lines. Results showed a significant reduction in spheroid size by EGCG-T-NPs, especially in $PSMA^+$ (22Rv1) cells. The targeted NPs significantly enhanced the antiproliferative activity of EGCG against PCa cell lines, especially toward the $PSMA^+$ cells, known to have higher FOLR1 expression. We did not observe any changes in the reactive oxygen species formation in both studied cell lines. However, significant changes in mitochondrial depolarization (15%) and polarization (18%) were recorded in response to EGCG-T-NP compared to control in 22Rv1. Similarly, EGCG-T-NP treatment also showed an increase in the number of dead apoptotic cells in 22Rv1 spheroids. Collectively, the obtained results support our hypothesis about the role of these targeted nanoprototypes in the increasing cellular uptake of EGCG payload into PCa cells, thus enhancing its antitumor efficacy.

Keywords: epigallocatechin gallate, folate receptor, molecular docking, nanoparticles, prostate cancer, targeted delivery

*** Corresponding author: Shams Tabrez,** King Fahd Medical Research Center, King Abdulaziz University, Jeddah, Saudi Arabia; Department of Medical Laboratory Technology, Faculty of Applied Medical Sciences, King Abdulaziz University, Jeddah, Saudi Arabia, e-mail: shamstabrez1@gmail.com
Read F. Alserihi: Department of Medical Laboratory Technology, Faculty of Applied Medical Sciences, King Abdulaziz University, Jeddah, Saudi Arabia; 3D Bioprinting Unit, Center of Innovation in Personalized Medicine, King Abdulaziz University, Jeddah, Saudi Arabia
Mohammed Razeeth Shait Mohammed, Mohammed Kaleem: Department of Biochemistry, Faculty of Science, King Abdulaziz University, Jeddah, Saudi Arabia
Mohammad Imran Khan: Department of Biochemistry, Faculty of Science, King Abdulaziz University, Jeddah, Saudi Arabia; Centre for Artificial Intelligence in Precision Medicines, King Abdulaziz University, Jeddah, Saudi Arabia
Mario Sechi: Department of Medical, Surgical and Experimental Sciences, Laboratory of Drug Design and Nanomedicine, University of Sassari, 07100 Sassari, Italy
Vanna Sanna: Nanomater s.r.l., 07041 Alghero, Italy
Torki A. Zughaibi, Adel M. Abuzenadah: Department of Medical Laboratory Technology, Faculty of Applied Medical Sciences, King Abdulaziz University, Jeddah, Saudi Arabia; King Fahd Medical Research Center, King Abdulaziz University, Jeddah, Saudi Arabia

1 Introduction

Prostate cancer (PCa) is the most common neoplastic disorder and the second leading cause of cancer-related deaths among males worldwide [1]. It accounts for 7.3% of all cancer incidences and 3.8% of cancer-related deaths in males in 2020 [2]. The increasing prevalence of PCa has become a global health challenge causing multi-organ spread and poorer prognosis in advanced stages [3]. Extra-prostatic or metastatic stage diagnosis and neoplastic heterogeneity often complicate the therapeutic benefits [4]. Therefore, there is a compelling requirement to discover novel, harmless yet highly specific chemotherapeutics against this type of cancer [5,6].

Green tea, the most popular beverage consumed worldwide, demonstrated various degrees of protection against

different diseases, including cancer [7,8]. An active catechin component, the (−)-epigallocatechin 3-gallate (EGCG), has shown an effective chemopreventive potential by modulating various cell signaling pathways in several *in vitro* assays of tumor cell lines and in *in vivo* preclinical, experimental models of induced carcinogenesis [9,10]. The first pioneering work highlighted that oral administration of green tea catechins extracts could be beneficial in the early stage of PCa, leading to a long-lasting inhibition of cancer progression [11,12]. Further data reported the therapeutic effectiveness of EGCG alone or in combination against PCa and other cancer [13,14]. Despite its efficacy and safety, the role of EGCG in cancer prevention and therapy is still discussed due to poor absorption, rapid metabolism and elimination, and inefficient systemic bioavailability [15].

In this context, nanotechnology-based strategies such as liposomes, nanoparticles (NPs), micelles, and other formulations have shown improvement in the anticancer potential of EGCG by enhancing its potency and reducing toxicity, side effects, and increased the concentration at the cancer site [16–18]. Advances in engineered nanovehicles with various materials allowed sustained delivery and controlled release of EGCG with enhanced stability and bioavailability [19,20]. Among these nanosystems, polymeric NPs are largely considered because of good biocompatibility, simple design, preparation, and customization, especially for targeted delivery [21,22]. Previously, Siddiqui *et al.* introduced the concept of "nanochemoprevention," where the efficacy of EGCG encapsulated in polylactic acid–polyethylene glycol NPs was determined in a preclinical setting [16,23,24]. A major challenge to improve the pharmacological profile of EGCG can also be pursued by a cell/tissue-specific targeting approach [25]. In our earlier studies, we developed novel NPs targeting prostate-specific membrane antigen (PSMA), a tumor-associated membrane receptor that appeared overexpressed in some specific PCa cells [26,27].

Active targeting exploited by the inclusion of a specific ligand on the NPs' surface is expected to provide an intriguing strategy for the development of effective antitumor therapeutics. In this study, we focused our attention on folate receptors human folate receptor alpha (FOLR1), well-known transmembrane glycoproteins, highly expressed on the majority of cancer tissues, to exploit the folate demand of rapidly dividing cells under low folate conditions [28,29]. Since PSMA has significantly elevated levels in prostate tissue compared with normal tissues, its upregulation contributed to tumor progression. PSMA exhibits the enzymatic function as a glutamate carboxypeptidase and folate hydrolase, thus implying its role in the metabolism of folates and their subsequent uptake [30].

Functionalization of NPs with ligands, *i.e.*, folic acid (FA), able to bind to the extracellular region of these receptors, can be considered for selective and effective delivery of ECGC to PCa cells. To the best of our knowledge, no previous study has shown the effect of EGCG-loaded PLGA–PEG–FA-based NPs in PCa cells using a 3D culture model. In the present study, we developed a precise targeted polymeric (PLGA–PEG) EGCG-loaded NPs, decorated with FA small molecules on their shell surface to achieve active cellular targeting toward FOLR1 and PSMA, and investigated their antiproliferative properties and compared the efficacy in two PCa cells (*i.e.*, PC3 [$PSMA^-$] and 22Rv1 [$PSMA^+$]). The reason for selecting PC3 and 22Rv1 was the presence (22Rv1) or absence (PC3) of PSMA, albeit both expressed FOLR1. On the other hand, choosing the 3D cell culture system over the traditional 2D model was due to its ability to better represent human tissues outside the body [31].

2 Materials and methods

2.1 Molecular modeling

The three-dimensional structure of the FOLR1 in complex with FA was retrieved from the RCSB Protein Data Bank (pdb: 4LRH, resolution: 2.80 Å) [32] utilizing a well-established docking protocol [33,34]. The docking studies were performed on a personal Macbook installed with the IOS operating system. The ligands FA and PEG–FA were constructed in a neutral form and energy was minimized by standard molecular mechanics protocols. The protein target was prepared by using AutoDock version 4.25 [35]. Briefly, ions and water molecules were removed, while hydrogen atoms were highlighted by the ADT module implemented in AutoDock. The charges were checked using the appropriate Gasteiger module for proteins implemented in AutoDock [36]. The docking was performed using the empirical free energy function and the Lamarckian protocol [37]. Mass-centered grid maps were generated with 40 grid points for every direction. Random starting position on the entire protein surface, orientations, and torsions were used for the ligands. Interactions in all the complexes were analyzed.

2.2 Chemistry of polymer synthesis

2.2.1 Chemistry

The synthesis of the copolymers was followed as described earlier with slight modification [38]. The analyses were done

by using different techniques such as nuclear magnetic resonance (^{1}H-NMR), MALDI-TOF mass spectra, UV-vis absorption spectra, and HPLC. The synthesized materials were found to be >95% pure.

2.3 Synthesis of PLGA–PEG–NH_2

We prepared a sufficient amount of activated PLGA–*N*-hydroxysuccinimide (NHS) intermediate. Briefly, NHS (32 mg, 1.1 mmol, ~4 equiv.) and 1-ethyl-3-(3-dimethylaminopropyl)-carbodiimide (58.2 mg, 1.2 mmol, ~4.3 equiv.) were added under nitrogen atmosphere to a solution of PLGA–COOH (1.25 g, 0.07 mmol) in anhydrous methylene chloride (5 mL). The resulting solution was magnetically stirred at room temperature for 12 h. The activated polymer of PLGA–NHS was collected by first precipitation with cold diethyl ether (5 mL) as a white solid, which was filtered and repeatedly washed in a cold mixture of diethyl ether and methanol. Then, the product was dried with nitrogen under vacuum to remove the solvent (yield: ~96%). In the next stage, DIPEA (0.18 mL, 1.034 mmol) was added to a solution of PLGA–NHS (0.10 g, 0.0056 mmol) in anhydrous $CHCl_3$ (2 mL) and NH_2–PEG–NH_2 (0.098 g, 0.028 mmol) in anhydrous $CHCl_3$ (1 mL). The solution was magnetically stirred at room temperature for 24 h under a nitrogen atmosphere. The PLGA–PEG–NH_2 copolymer was obtained by precipitation with cold diethyl ether, dried under vacuum, and used to synthesize the PLGA–PEG–FA copolymer without further treatment (yield, 92%). ^{1}H-NMR (400 MHz, $CDCl_3$): δ 5.30–5.12 (m, 1H, –OC–CH(CH_3)O–, PLGA), 4.90–4.62 (m, 2H, –OC–CH_2O–, PLGA), 3.65 (brs, 2H, –CH_2CH_2O–, PEG), 1.58 (brs, 3H, –OC–CH(CH_3)O–, PLGA) [38].

2.4 Synthesis of FA–NHS intermediate

The activated FA was synthesized as per the earlier study with few modifications [39]. FA (100 mg; 0.226 mmol), DCC (93.5 mg; 0.453 mmol, 2 equiv.), and NHS (52.08 mg; 0.453 mmol, 2 equiv.) were dissolved and magnetically stirred under light protection and in nitrogen atmosphere in 1.5 mL dimethyl sulfoxide (DMSO) in the presence of a catalytic amount of triethylamine (TEA; 0.045 mL) for 16 h. Then, the reaction mixture was filtered, and the solution was repeatedly treated (decantation and filtering) with cold anhydrous ether to obtain a yellow/orange product. FA–NHS was fully characterized using NMR and mass spectrometry.

2.5 Synthesis of PLGA–PEG–FA

PLGA–PEG–NH_2 (500 mg; 0.02736 mmol) and FA–NHS (36.25 mg; 0.08208 mmol) were dissolved in 5 mL DMSO, and the resulting reaction was stirred for 24 h under light-protected conditions in argon atmosphere [39]. The desired tri-block-copolymer was obtained as a solid after precipitation with cold methanol, diethyl ether. The solid was filtered and dried under a vacuum to obtain a crude orange powder. Then, the product was dissolved in 80 mL of dichloromethane (DCM) and filtered, and the solution was concentrated to obtain an amorphous solid, which was used for the preparation of targeted NP (yield, 69%). ^{1}H-NMR (400 MHz, $CDCl_3$): δ 5.28–5.12 (m, –OC–CH(CH_3)O–, PLGA), 4.98–4.85 (m, –OC–CH_2O–, PLGA), 3.5 (brs, –CH_2CH_2O–, PEG), 1.48 (brs, –OC–CH(CH_3)O–, PLGA). The characteristic pattern of FA (6.6–6.7 ppm, 7.6–7.7 ppm, and 8.6–8.7 ppm) was detected in the spectra.

2.6 Preparation of NPs

NPs were prepared using a nanoprecipitation method as reported earlier with slight modifications [27]. Unloaded NPs were also formulated and used for comparison (vehicle control, Ø-T-NP).

2.7 Characterization of NPs

2.7.1 Morphology and size

Morphological examination of NPs was conducted by utilizing environmental scanning electron microscopy (Zeiss LS10, Germany). Operatively, a drop of an aqueous suspension of NPs was deposited on an aluminum stub and dried until complete solvent (water) evaporation. Then, the samples were submitted to gold sputtering (Sputter Coater Edwards S150A) and analyzed at an acceleration voltage of 10 kV under an argon atmosphere. Mean diameter and polydispersity index (PDI) of NPs were measured using photon correlation spectroscopy (Zetasizer

Nano ZS, Malvern Instruments, UK) at 25°C and at a scattering angle of 90° after dilution of samples with Milli-Q water. Each sample was measured in triplicate.

2.7.2 Drug loading content, encapsulation efficiency, and production yields

The amount of the loaded EGCG was determined by dissolving a weighed amount of dried EGCG-loaded NPs in a mixture of acetonitrile/water (50:50, v/v) using a modified HPLC method [40]. Chromatographic analysis was performed on a 1260 Infinity II (Agilent Technologies, US) liquid chromatography system equipped with a diode array detector of the same series, using an Infinity Lab Poroshell 120, EC-C18 column (4 µm, 4.6 mm × 100 mm; Agilent Technologies) with an elution flow rate of 0.8 mL/min, and a linear solvent gradient of A–B [(A, 10 mM KH_2PO_4 (pH 4.0); B, CH_3CN:H_2O (65:35 v/v)], as follows: 0 min, 0% B; 5 min, 20% B; 15 min, 30% B.

The injection volume was 20 µL, the wavelength for UV detection was 280 nm, and the retention time of EGCG was 11 min. The calibration curves were found to be linear in the range of 12.5–100 µg/mL ($y = 30.453x$; $R^2 = 0.9999$). The production yields were reported and expressed as the weight percentage of the weighed product after drying, considering the initial amount of solid materials used for the preparation of NP.

2.8 Biological evaluation

2.8.1 Cell culture

Tumorigenic cell lines, namely, PC3 and 22Rv1 (prostate carcinoma), were procured from ATCC (Manassas, VA, USA). ATCC used a short tandem repeat DNA profiles database for their identity confirmation. Both cell lines were cultured in a suitable cell culture medium, *i.e.*, DMEM and RPMI-1640 (Gibco, ThermoFisher, USA), respectively, containing 10% fetal bovine serum and 1% penicillin.

2.8.2 3D spheroid assay

We cultured both cell lines on poly-HEMA-covered plates for different time points for the induction of 3D assay. Once formed, the spheroids were treated with either empty targeted nanoparticles (Ø-T-NPs) or with EGCG-targeted nanoparticles (EGCG-T-NPs) continuously for 6 days. The spent media was replaced with fresh media every 2 days. The images of spheroids were captured by using Nikon inverted light microscope, and images were analyzed for size measurement by image J software (https://image j.net/Invasion assay).

2.8.3 Reactive oxygen species measurement in spheroids

CellROX (Life Technologies, Carlsbad, CA, USA) dye was used to quantitate the amount of reactive oxygen species (ROS) formation in spheroids. For ROS quantification, both cell lines were plated on poly-HEMA-coated six-well plates treated with either Ø-T-NP or EGCG-T-NP continuously for 6 days. After reaching the time point, CellROX (500 nM) was added and incubated at 37°C in 5% CO_2 for 60 min. After the incubation, the samples were analyzed using a flow cytometer at 488 nm excitation for the CellROX® Green.

2.8.4 Mitochondrial membrane potential measurement in spheroids

For the mitochondrial membrane potential (MMP) analysis, the spheroids were treated with either Ø-T-NP or EGCG-T-NP continuously for 6 days using the procedure described by Mittal *et al.* [41]. The cells were analyzed for red and green fluorescence in a flow cytometer (Guava easyCyte™ Luminex) coupled with 485 nm excitation filter and 590 nm emission filter.

2.8.5 Live dead assay in spheroids

For this assay, the spheroids were either treated with Ø-T-NP or EGCG-T-NP continuously for 6 days. After completion of the time point, the spheroids were washed with 1× PBS and incubated with 10 µg/mL of propidium iodide (PI) dye in culture medium for 10 min at 37°C. The cells were then analyzed for red fluorescence in a flow cytometer (Guava easyCyte™ Luminex).

3 Statistical analysis

Differences between vehicle control and EGCG targeted NPs treated groups were determined by one-way analysis of variance for multiple groups, using GraphPad Prism 8.0 software (GraphPad Software, La Jolla, CA, USA).

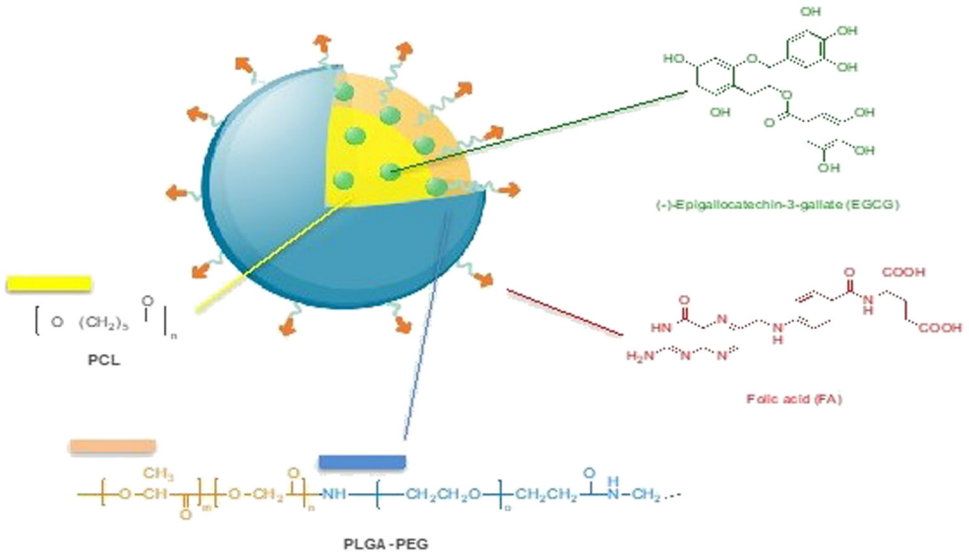

Figure 1: Schematic representation of the designed targeted PLGA–PEG–FA-based (EGCG)-loaded NPs (EGCG-T-NPs). Chemical structure of EGCG, FA targeting ligand, and PLGA–PEG/PCL polymers.

Test results with $P < 0.05$ were considered statistically significant.

4 Results

4.1 Design of FA-targeted NPs

We envisioned obtaining novel FA-targeted polymeric NPs encapsulated with EGCG (EGCG-T-NPs) (Figure 1). A blend of poly(D,L-lactide-*co*-glycolide) poly(ethylene glycol) (namely, PLGA–PEG) and poly(epsilon-caprolactone) (PCL) was considered as biocompatible/biodegradable polymeric mixture. We used the di-block-copolymer PLGA–PEG–NH_2 intermediate to conjugate the FA and obtain the tri-block-copolymer PLGA–PEG–FA, needed for the preparation of targeted NPs.

To get information on the impact of FA-PEGylation in primary binding with FOLR1, we conducted a comparative computational docking study between FA (pdb: 4LRH) and a model of PEG–FA to the FOLR1 catalytic site, and peculiar ligand–protein interactions and the docking binding energies were analyzed. Docking analysis revealed that both FA and PEG–FA overlapped and accommodated well within the active site (Figure 2). In contrast, the polymeric aliphatic model (PEG–FA) showed slightly better docking energy to FA binding with FOLR1 (docking energies were –13.232 and –14.126 kcal/mol, for FA and PEG–FA, respectively). More specifically, the folate pteroate moiety was placed inside the receptor, whereas its glutamate moiety extends externally from the cavity to the solvent, sticking out of the pocket entrance, especially the conjugated model. The X-ray cocrystal structure showed stacking of the pterin ring between a pocket formed by Asp81, Tyr85, Trp171, and Ser174 residues, whereas the aminobenzoate portions of both ligands shared hydrophobic interactions with His135, while the glutamate moieties formed hydrogen bonds with Trp102, Gly137, and Trp140. Further interactions with His135, Gly137, and Trp138 contributed to stabilizing the aminobenzoate backbone. This observation supported the use of the PEG–FA constructs for this study.

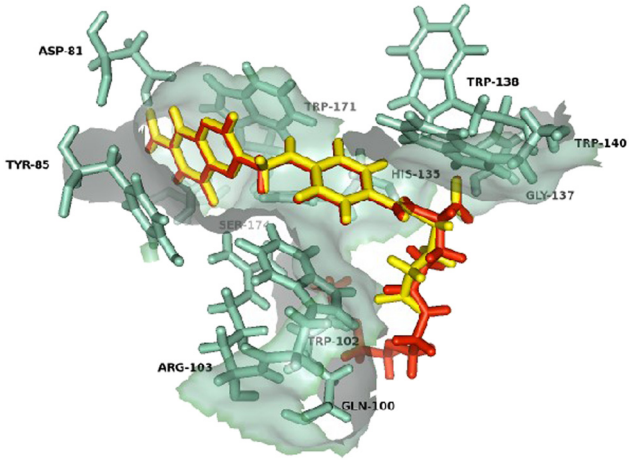

Figure 2: Binding modes of both FA (yellow) and its PEG polymeric conjugated (PEG–FA) model (red) superimposed on the folate receptor active site (pdb: 4LRH).

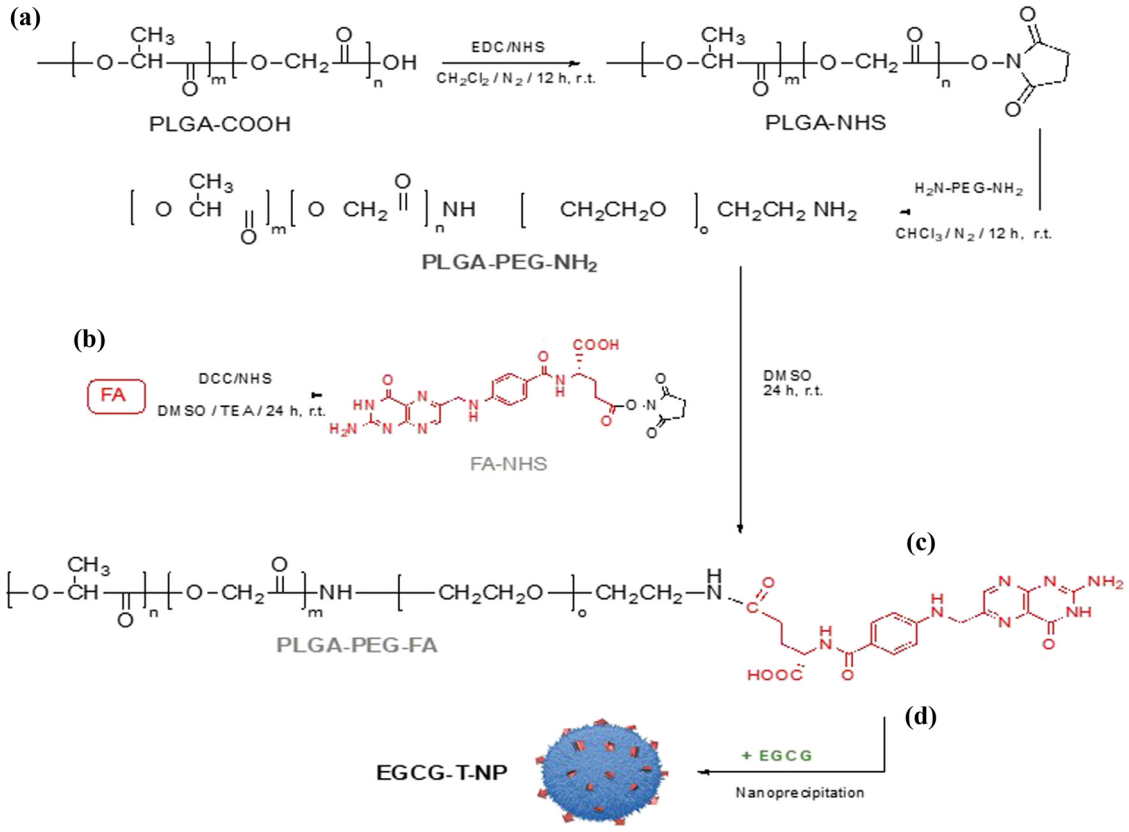

Scheme 1: (a) Synthesis of copolymer PLGA–PEG–NH_2, (b) FA–NHS intermediate, (c) tri-block-copolymer PLGA–PEG–FA, and (d) nano-formulation for EGCG-T-NP.

4.2 Synthesis of tri-block-copolymer PLGA–PEG–FA

The PLGA–PEG–FA tri-block-copolymer was synthesized using a two-step reaction, as described earlier (Scheme 1a–c). First, the carboxyl-terminus PLGA–COOH was activated (with NHS) to generate the intermediate PLGA–NHS, which was then converted on PLGA–PEG–NH_2 by conjugating bifunctional PEG, NH_2–PEG–NH_2, to activated polymer (Scheme 1a). The structure of the copolymer was confirmed by ^{1}H-NMR spectroscopy. More specifically, a signal detected at 1.48 ppm was attributed to the lactide methyl repeat units. Overlapping multiplets observed in the range of 5.30–5.15 and 4.96–4.80 indicated the lactide methine and the glycolide protons, respectively. Moreover, in addition to the signals specific for PLGA, the presence of the peak at about 3.51 ppm correspond to the PEG methylene protons, confirming the successful preparation of the desired copolymer. The desired PLGA–PEG–FA was obtained by conjugating the activated targeting agent, *i.e.*, FA–NHS (Scheme 1b), to the amine PEG terminal group of PLGA–PEG–NH_2, which resulted in the structurally and physiologically stable amide bonds (Scheme 1c). The presence of the folate terminal groups was confirmed by ^{1}H-NMR analysis, which displayed the PLGA pattern in the range of 5.1–5.3, 4.8–5, and 1.5 ppm, while the PEG moiety was detected at 3.5 ppm. The characteristic peaks of the folate termini were found to be at 6.6–6.7 ppm, 7.6–7.7 ppm, and 8.6–8.7 ppm, supporting the successful conjugation (Figure 3).

4.3 Preparation and characterization of NPs

NPs were successfully obtained by the nanoprecipitation technique using a blend of hydrophobic polymer PCL and the amphiphilic block copolymers PLGA–PEG–FA (Scheme 1d). We prepared two batches of NPs, which included PLGA–PEG–FA loaded with EGCG NPs (EGCG-T-NPs), and its unloaded ones (Ø-T-NP) for comparison. The blended approach allows the hydrophobic PLGA component and PCL self-assembly to form a core surrounded by hydrophilic PEG chains, thus provide better hydrophilic/hydrophobic balancing. These polymers, particularly PEG, confer a hydrophilic surface to NPs, which provide antibiofouling properties, prevent/reduce nonspecific interaction, and limit macrophage capture. PEG was also able to ensure the

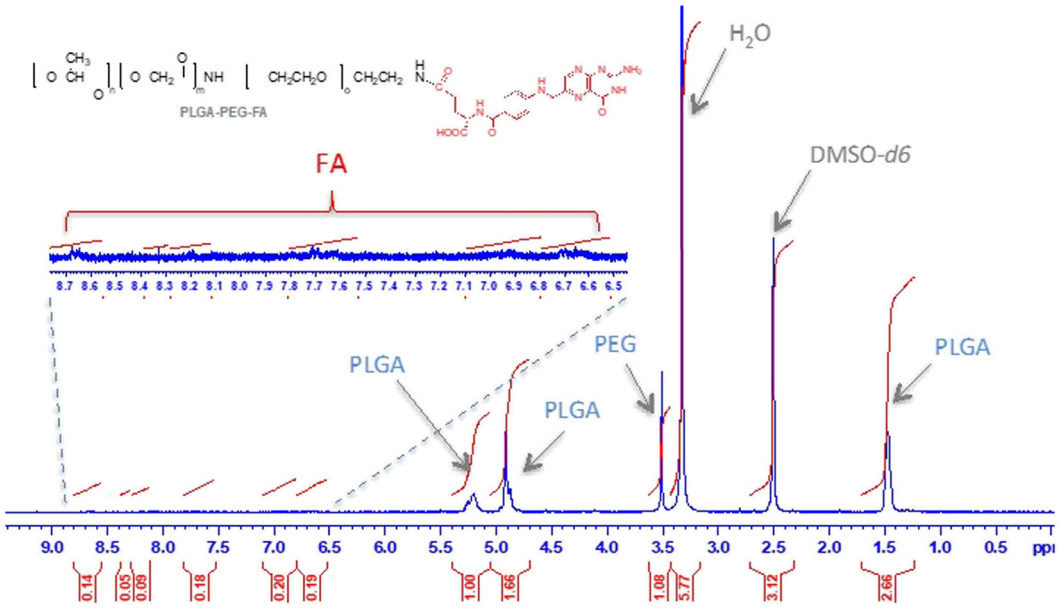

Figure 3: ^{1}H-NMR characterization of copolymer PLGA–PEG–FA.

optimal distance between FA and NP surface. Conversely, PEGylation allows enhanced distribution and prolonged circulation time of NPs in blood by improved permeability and retention (EPR) effect, resulting in increased accumulation in tumors.

The scanning electron microscope (SEM) observations showed that both NPs batches have well-dispersed particles with a regular spherical shape (Figure 4). The particle size of NPs ranges from 115 nm to about 130 nm, suggesting that the loading of the EGCG into NPs did not result in a significant increase in size compared to the corresponding free counterparts (Table 1). The NP dispersions were characterized by low PDI values (below 0.2), indicating a narrow and unimodal distribution, typical behavior of monodispersed systems (Figure 1). As far as the drug entrapment efficiencies were concerned, the encapsulation efficiency of EGCG-T-NP was found to be 50%, suggesting a good affinity of polymeric blend with the EGCG molecules. Moreover, yields of production obtained were high and were found to be in the range of 75–82%.

4.4 EGCG-targeted nanoparticle treatment reduces spheroid size of PCa cell lines

3D spheroids are well-established mimics of *in vivo* tumors; therefore, we used this highly important and specific model to assess the antitumorigenic capacity of EGCG-targeted NPs. We assessed the impact of both empty targeted NP and EGCG-targeted NP treatment on spheroids size of two well-known PCa cell lines, namely, 22Rv1 and PC3. As

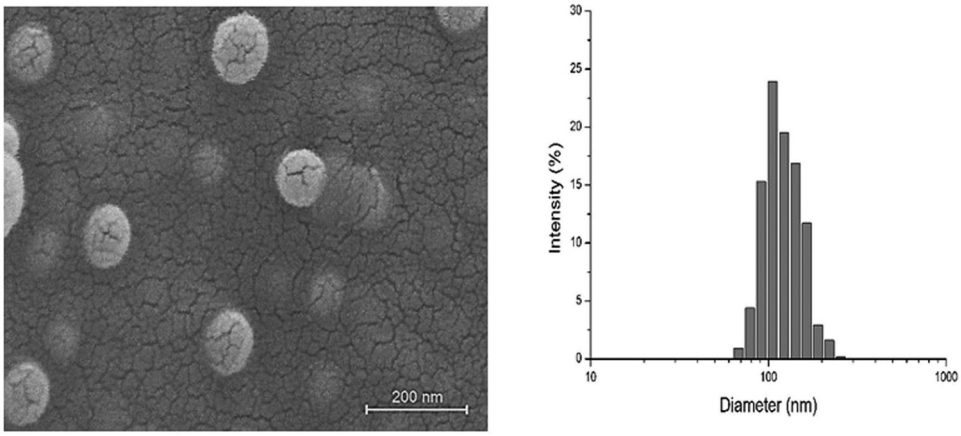

Figure 4: SEM images of EGCG-T-NP (left) and corresponding particle size distribution (right). The scale bar is 200 nm.

Table 1: Average diameter, PDI, percentage of EE, EGCG loading content (DLC%) ±, and YP% of formulated NPs. Data are represented as mean ± SD, $n = 3$

Batch	Mean diameter (nm)	PDI	EE (%)	DCL (%)	YP (%)
Ø-T-NP	115.28 ± 6.17	0.123 ± 0.04	—	—	75.60 ± 3.06
EGCG-T-NP	128.42 ± 3.57	0.114 ± 0.03	49.82 ± 3.74	2.49 ± 0.19	81.73 ± 6.21

shown in Figure 5(a and b upper panel), detachment of both 22Rv1 and PC3 cell lines results in a statistically significant and gradual increase in spheroid size in the presence of empty targeted NP, *i.e.*, from 183 mm^3 on the second day to 245 mm^3 on the sixth day in 22Rv1 cells and from 236 mm^3 on the second day to 438 mm^3 on the sixth day in PC3 cells. However, treatment with EGCG-targeted NPs significantly reduces the spheroid size on the sixth day, *i.e.*, from 245 to 96 mm^3 in the 22Rv1 cell line (Figure 5a, lower panel). Furthermore, we observed a similar decrease in the spheroid size on the second day and from 438 to 370 mm^3 on the sixth day (Figure 5b, lower panel) in the PC3 cell line. Overall, the aforementioned data clearly showed that EGCG-targeted NP significantly attenuates spheroid formation of detached 22Rv1 cells compared to PC3 cells.

4.5 EGCG-targeted nanoparticle treatment fails to induce ROS in spheroids of PCa cell lines

We assessed the impact of both empty targeted NPs and EGCG-targeted NPs treatment on ROS production in spheroids of both studied cell lines. As shown in Figure 6(a and b, upper and lower panels), EGCG-targeted NP treatment fails to induce any significant production of ROS in both 22Rv1 and

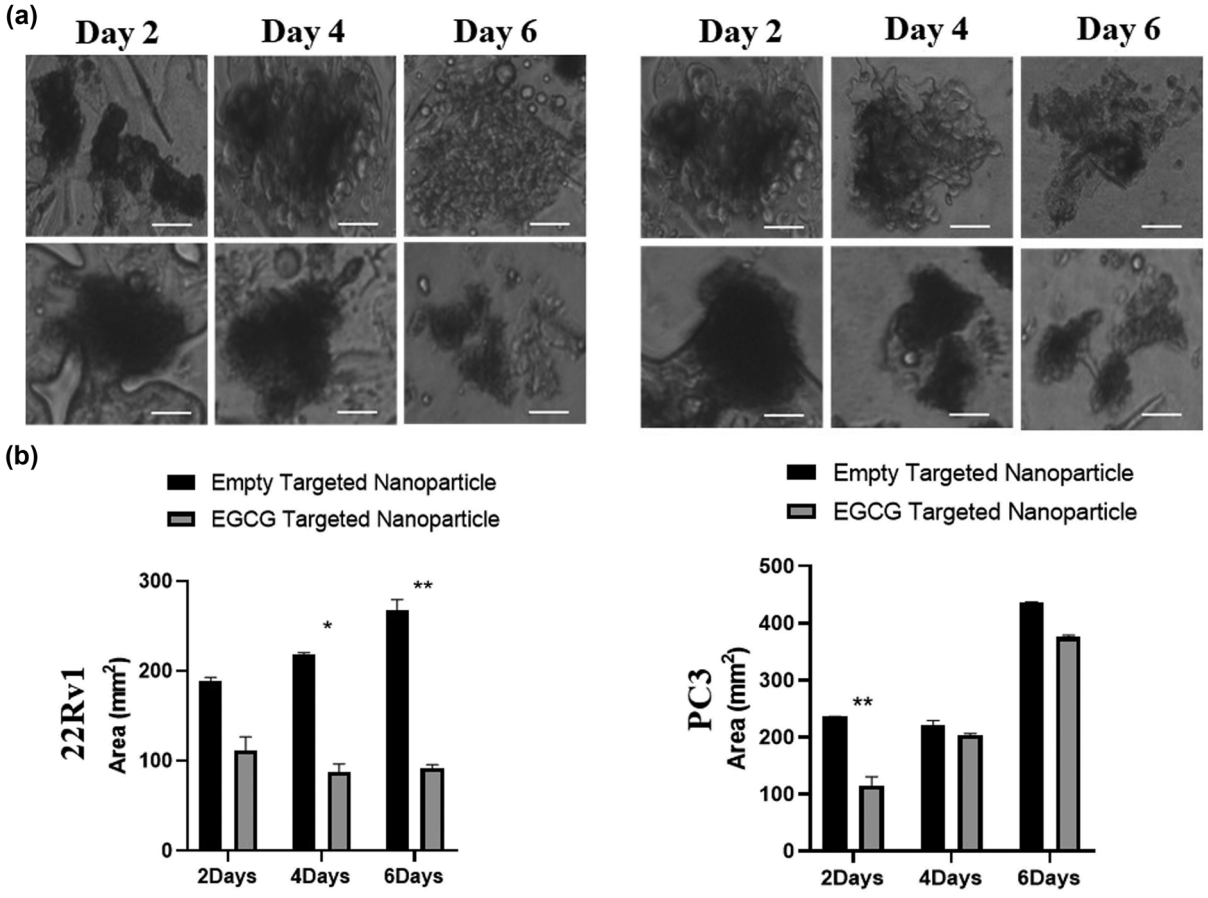

Figure 5: EGCG-targeted nanoparticle decreases spheroid size. Both (a) 22Ru1 and (b) PC3 were fully grown in poly-HEMA-coated plates to form 3D spheroids. Furthermore, spheroids were treated with empty targeted nanoparticle or EGCG-targeted nanoparticle for 2–6 days, and pictures were taken by Nikon inverted light microscope at ×40. Images were analyzed for size measurement using image J software (mean ± S.E.M., $n = 100$). *$P < 0.05$, **$P < 0.01$, and ***$P < 0.001$. A total number of 100 spheroids were measured for size examination.

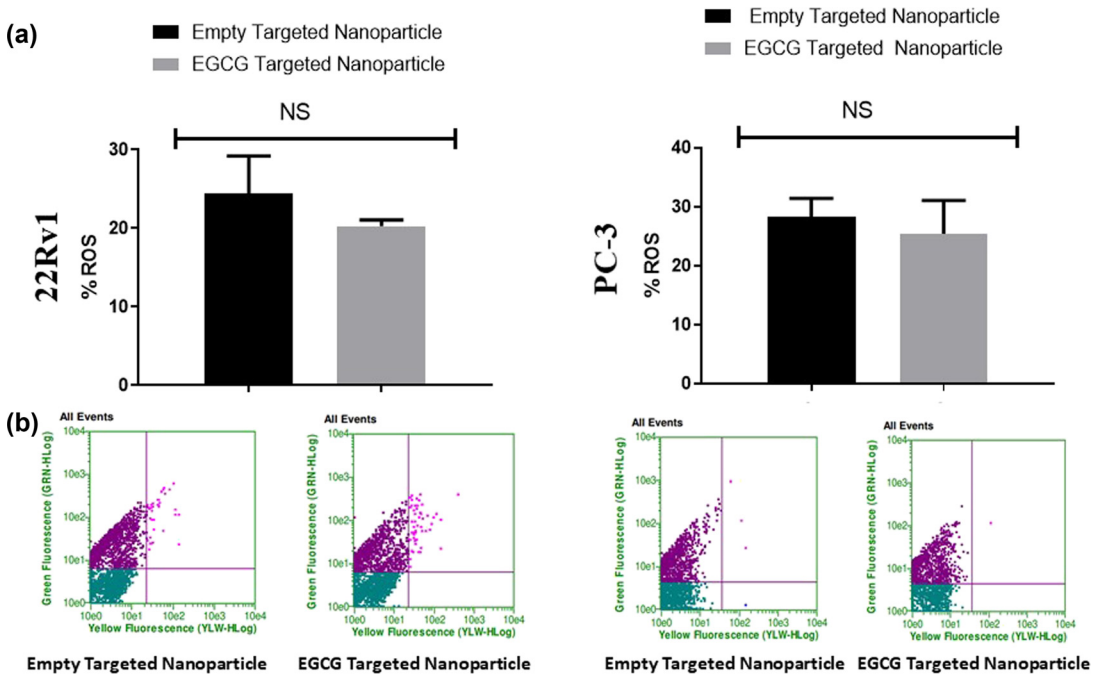

Figure 6: EGCG-targeted nanoparticle fails to induce ROS in spheroids of PCa cell lines. Both (a) 22Rv1 and (b) PC-3 were grown on poly-HEMA-coated plates and treated with either empty targeted nanoparticles or EGCG-targeted nanoparticle (6 μM) for 6 days. At the end of the time point, CellROX dye was added to the spheroids and incubated for 30 min in dark. Fluorescent intensity was measured by using Guava Flow Cytometer at a standardized wavelength provided by the manufacturer. Values are shown as mean ± SEM (n = 6).

PC3 cell lines compared to empty targeted NPs. These results suggest that the antitumorigenic capabilities of EGCG-targeted NPs were devoid of ROS-mediated mechanism(s).

4.6 EGCG-targeted nanoparticle treatment promotes mitochondrial leakage and cell death

The spheroids of 22Rv1 treated with empty targeted NPs and EGCG-targeted NPs showed a significant ($P < 0.001$) increase in mitochondrial depolarization. The EGCG-targeted NPs reduce polarization in the mitochondrial membrane in 22Rv1, but no significant difference was observed in PC3 cells as evident by JC-1 dye fluorescence (Figure 7, upper and lower panels). Results showed an approximately 18% reduction in mitochondrial polarization and a 15% increase in mitochondrial depolarization in 22Rv1 spheroids treated with EGCG-targeted NPs compared to empty targeted NPs. Both increases in depolarization and decreases in the polarization of mitochondria membrane potential are hallmarks of mitochondria-mediated apoptosis. As evident in Figure 8 (upper and lower panels), the number of dead apoptotic cells was also found to be increased in 22Rv1 spheroids treated with EGCG-targeted NPs compared to empty targeted NPs. An approximately 12% increase in apoptotic cells was observed in 22Rv1 treated with EGCG-targeted NPs compared to control NPs. Conversely, we did not observe any significant difference in the number of dead apoptotic cells with respect to both control and EGCG-targeted NPs in PC3 cells.

5 Discussion

The quest of a potential anticancer agent marks the polyphenolic constituent of green tea, viz, EGCG. Despite its therapeutic potential over a wide range of cancer, its clinical application has been limited because of the low utilization rate with poor stability and systemic bioavailability [42–44]. Deprived intestinal stability and low absorption were suggested as the main culprits that influenced its bioavailability [45]. In addition, the lack of specific receptors carrying EGCG into cells and the presence of efflux proteins that pump back EGCG into the intestinal lumen also result in reduced absorption of

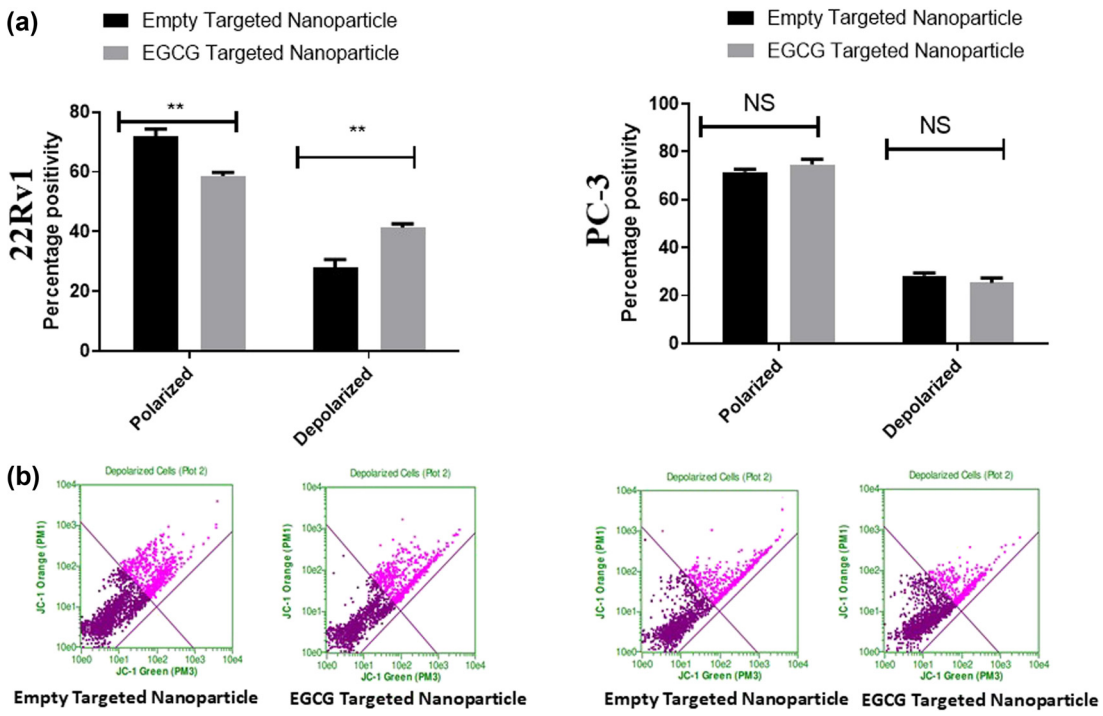

Figure 7: EGCG-targeted nanoparticle induces depolarization in spheroids. Both 22Rv1 (a) and PC3 (b) were grown on poly-HEMA-coated plates and treated with either empty targeted nanoparticles or EGCG-targeted nanoparticles (6 μM) for 6 days. At the end of time point, JC-1 dye was added to the treated spheroids and incubated for 30 min at 37°C. Fluorescent intensity was measured using Guava Flow Cytometer at the standardized wavelength provided by the manufacturer. Values are shown as mean ± SEM (n = 6). *P < 0.05, **P < 0.01, and ***P < 0.001.

EGCG in cells [45,46]. Several approaches have been reported in the scientific literature to overcome the reduced bioavailability of EGCG in the therapeutic setup. Earlier works reported significantly increased bioavailability of EGCG by molecular modifications, nanostructure-based drug delivery systems, and the co-administration of EGCG with other bioactive compounds [19,45]. Nanostructure-based drug delivery systems have been suggested as a potential approach that helps to overcome the stability and bioavailability of the enclosed EGCG.

In this study, we used a biocompatible block-copolymer PLGA–PEG–FA for the preparation of targeted EGCG-loaded NPs. A blend of poly(D,L-lactide-*co*-glycolide) poly(ethylene glycol) (namely, PLGA–PEG) and PCL was considered as biocompatible/biodegradable polymeric mixture for the preparation of NPs [47]. These are the widely considered polyesters for building the core of polymeric micelles and have shown great promises as potential nanocarriers [48]. Compared to other polymeric esters, PCL degradation proceeds very slowly, limiting its utilization in some specific biomedical fields. Modification such as surface decoration or forming composite systems with other natural and synthetic polymers make PCL suitable for a larger application [49,50]. The blended approach allows the hydrophobic PLGA block and PCL self-assembly to form a core surrounded by hydrophilic PEG chains, thus providing a better hydrophilic/hydrophobic balancing. Previously, we reported a precisely controllable EGCG loading content, better encapsulation efficiency, and high production yields by a blend of two polymers, PLGA–PEG–A or PLGA–PEG–DCL, or PLGA–PEG–AG, with PCL [27].

Diverse tumor tissue targeting approaches have been reported in the literature for an accurate and effective anticancer therapy of small molecules [18]. The aggressive upregulation of high-affinity folate receptors in PCa cells with a limited expression in nonmalignant cells makes it an important targeting molecule [51]. The increase in folate receptors reflects the increased nutritional requirement of FA, which is essential for synthesizing nucleotide bases. Several studies suggested folate receptor targeting, a very promising approach in anticancer treatment [49–51]. The reduced off-site toxicity, increased selectivity, and enhanced potency by folate-tagged bioactive molecules against tumor cells compared to nontargeted drugs has been reported in the scientific literature [52–54]. EGCG combined with FA has also been reported for the chemopreventive effect on gastrointestinal carcinogenesis in rats [55]. Several studies also reported FA-conjugated nano

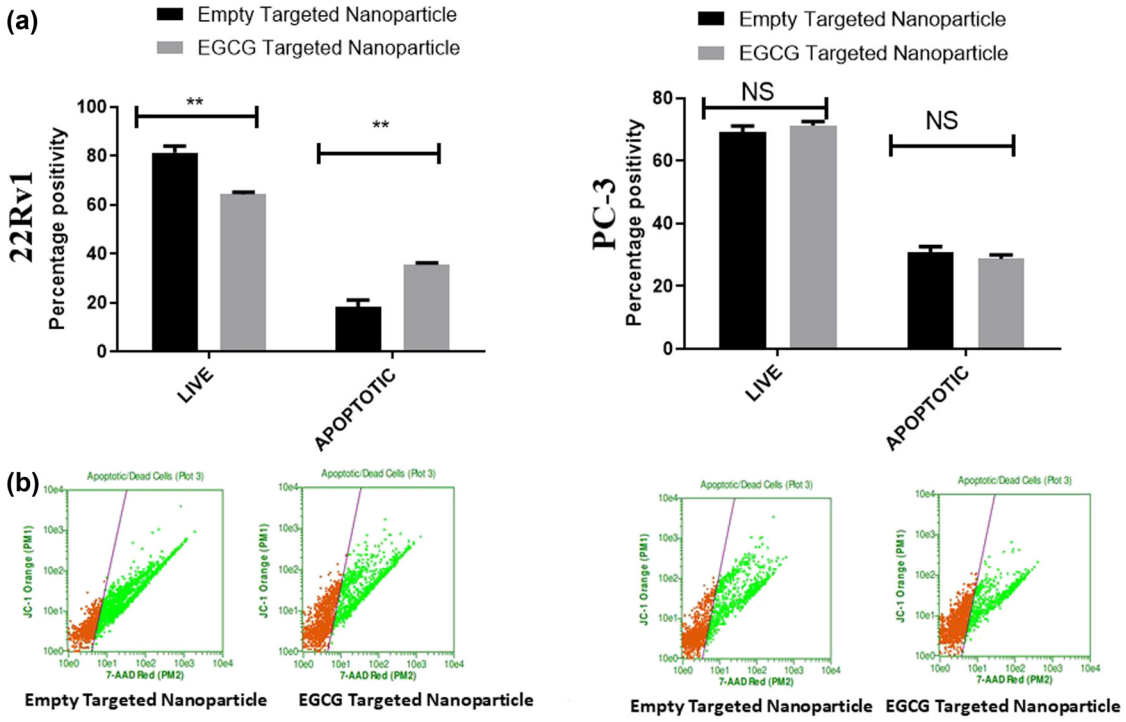

Figure 8: EGCG-targeted nanoparticle induces apoptosis in spheroids. Both 22Rv1 (a) and PC3 (b) were grown on poly-HEMA-coated plates and treated with either empty targeted nanoparticles or EGCG-targeted nanoparticles (6 μM) for 6 days. At the end of time point, PI dye was added to the treated spheroids and incubated for 30 min at 37°C. Fluorescent intensity was measured using Guava Flow Cytometer at standardized wavelength provided by the manufacturer. Values are shown as mean ± SEM ($n = 6$). *$P < 0.05$, **$P < 0.01$, and ***$P < 0.001$.

delivery systems as a promising way to improve the stability, solubility, bioavailability, and bioefficacy of EGCG compared to free EGCG [56–58]. One study suggested folate conjugation for tumor targeting by chitosan-coated EGCG NPs [56]. The high stability and smaller particle size are achieved by FA–PEG–NPs that provide higher intracellular uptake of EGCG than its free counterpart [57]. A folate peptide decorated PLGA NPs loaded with EGCG reported to strongly bind folate receptor-specific breast cancer cells (MDA-MB-231) to inhibit the progress of breast adenocarcinoma [58]. In an earlier study, Siddiqui *et al.* [16] reported a 10-fold dose advantage by PLA–PEG–EGCG NPs that showed pro-apoptotic and anti-angiogenesis effects in human PC3 cells.

Lately, the 3D cell culture model has gained attention in preclinical studies because of the possibility of screening a large number of different molecules [59]. This method typically uses an extracellular matrix (ECM) and can mimic cell-to-cell and cell-to-ECM interactions, including paracrine signaling [60]. In the 3D cell culture method, the cells grow in the 3D plane, aggregate, and self-assemble in an environment that prevents attachment to a flat surface, resulting in spheroid formation, which is well-established mimics of *in vivo* tumors [61]. The 3D tumor spheroids study model often provides comparable results to animal models in many aspects [62]. The predictability of 3D spheroids on *in vivo* efficacy could resolve the high cost and ethical issues associated with animal usage. It is well known that the spheroid growth impacts cell proliferation, apoptosis, and necrotic/hypoxic core formation, with the outer layer mostly proliferative, the middle layer hypoxic, and the inner core necrotic [63].

The size of tumors is regarded as a crucial factor in determining the drug penetration ability as the larger tumors lead to an increased resistance, which is also observed in 3D tumor spheroid models [64]. We observed a dramatic decrease in the spheroid size as a result of EGCG-targeted NP treatment in 22Rv1 compared to PC3 cell line. Similar results were observed by different research groups using PLGA/lipid NPs in 3D models [63,65,66]. In one study, PLGA-modified NP exhibited increased penetration and distribution in HeLa and SiHa HD spheroids [63]. Another study reported deep penetration by PLGA-encapsulated EtNBS NPs into the hypoxic and acidic cores (usually unresponsive tumor region) of 3D spheroid of gastrointestinal carcinoma [65]. One study reported better growth inhibition by verteporfin-encapsulated lipid nanocarriers compared to a

free drug in ovarian spheroid cancer cells [66]. Likewise, biotin-conjugated pullulan acetate NPs treatment also showed similar antitumor activity in 3D culture and xenograft hepatic tumor model [67]. Similar efficacy and deep tumor penetration with reduced tumor growth were reported in both SH-SY5Y spheroids and H22 tumor-bearing mice treated with iRGD-conjugated NPs with doxorubicin [68].

The current study did not observe any induction in ROS production by EGCG-targeted NP treatment in both studied cell lines. These results suggest that the observed antitumorigenic capabilities of EGCG-targeted NPs were devoid of ROS-mediated mechanism(s). Several studies also reported the anticancer activity of bioactive molecules by ROS-independent mechanism [69–71]. These evidence suggest that ROS are not obligator effectors in the anticancer mechanisms including apoptosis. This result clearly indicates the better efficacy of EGCG-T-NP toward 22Rv1 compared to PC3. The current result also highlights the strong dual binding of EGCG-T-NP with FOLR1 and $PSMA^+$ in 22Rv1. This was expected because of the presence of $PSMA^+$ and overexpression of FOLR1 in 22Rv1 cells. Mitochondrial metabolism has been reported to play a critical role in tumorigenesis and cancer development [72]. MMP is a key indicator of mitochondrial activity that reflects the process of electron transport and oxidative phosphorylation [73]. We observed increased depolarization and reduced polarization in the mitochondrial membrane potential after the treatment of EGCG-T-NPs in 22Rv1. The mitochondrial membrane depolarization has been reported to induce apoptosis [74]. Our results support earlier findings where increased proton influx leads to ROS production suppression during spontaneous transient depolarization [75]. Moreover, uncoupling of mitochondrial oxidative phosphorylation could also play a role in suppressing ROS production [76]. The current study also reported an increase in the number of dead apoptotic cells in 22Rv1 spheroids treated with EGCG-targeted NPs.

6 Conclusion

Overall, our results clearly indicate the successful synthesis of EGCG-loaded NPs that have the potential to bind FLOR1 and $PSMA^+$ dually. Because of the presence of $PSMA^+$ and overexpression of FLOR1, 22Rv1 showed better efficacy on the targeted delivery compared with PC3 cells ($PSMA^-$). We also observed a significant dose advantage by this EGCG-loaded NPs, indicating their anticancer potential at clinically relevant doses. Further, preclinical *in vivo* studies are recommended to verify *in vitro* data.

Funding information: The authors extend their appreciation to the Deputyship for Research & Innovation, Ministry of Education in Saudi Arabia for funding this research work through the project number 986.

Author contributions: All authors have accepted responsibility for the entire content of this manuscript and approved its submission.

Conflict of interest: The authors state no conflict of interest.

References

[1] Siegel RL, Miller KD, Fuchs HE, Jemal A. Cancer statistics, 2021. CA Cancer J Clin. 2021;71(1):7–33.
[2] Sung H, Ferlay J, Siegel RL, Laversanne M, Soerjomataram I, Jemal A, et al. Global cancer statistics 2020: GLOBOCAN estimates of incidence and mortality worldwide for 36 cancers in 185 countries. CA Cancer J Clin. 2021;71(3):209–49.
[3] Merriel SWD, Funston G, Hamilton W. Prostate cancer in primary care. Adv Ther. 2018;35(9):1285–94.
[4] Omabe K, Paris C, Lannes F, Taïeb D, Rocchi P. Nanovectorization of prostate cancer treatment strategies: a new approach to improved outcomes. Pharmaceutics. 2021;13(5):591.
[5] Oves M, Aslam M, Rauf MA, Qayyum S, Qari HA, Khan MS, et al. Antimicrobial and anticancer activities of silver nanoparticles synthesized from the root hair extract of Phoenix dactylifera. Mater Sci Eng C Mater Biol Appl. 2018;89:429–43.
[6] Shait Mohammed MR, Ahmad V, Ahmad A, Tabrez S, Choudhry H, Zamzami MA, et al. Prospective of nanoscale metal organic frameworks [NMOFs] for cancer therapy. Semin Cancer Biol. 2021;69:129–39.
[7] Surh Y-J. Cancer chemoprevention with dietary phytochemicals. Nat Rev Cancer. 2003;3(10):768–80.
[8] Mukhtar H. Chemoprevention: making it a success story for controlling human cancer. Cancer Lett. 2012;326(2):123–7.
[9] Du G-J, Zhang Z, Wen X-D, Yu C, Calway T, Yuan C-S, et al. Epigallocatechin gallate (EGCG) is the most effective cancer chemopreventive polyphenol in green tea. Nutrients. 2012;4(11):1679–91.
[10] Tabrez S, Jabir NR, Adhami VM, Khan MI, Moulay M, Kamal MA, et al. Nanoencapsulated dietary polyphenols for cancer prevention and treatment: successes and challenges. Nanomedicine (Lond). 2020;15(11):1147–62.
[11] Bettuzzi S, Brausi M, Rizzi F, Castagnetti G, Peracchia G, Corti A. Chemoprevention of human prostate cancer by oral administration of green tea catechins in volunteers with high-grade prostate intraepithelial neoplasia: a preliminary report from a one-year proof-of-principle study. Cancer Res. 2006;66(2):1234–40.

[12] Brausi M, Rizzi F, Bettuzzi S. Chemoprevention of human prostate cancer by green tea catechins: two years later. A follow-up update. Eur Urol. 2008;54(2):472–3.
[13] Johnson JJ, Bailey HH, Mukhtar H. Green tea polyphenols for prostate cancer chemoprevention: a translational perspective. Phytomedicine. 2010;17(1):3–13.
[14] Shin CM, Lee DH, Seo AY, Lee HJ, Kim SB, Son W-C, et al. Green tea extracts for the prevention of metachronous colorectal polyps among patients who underwent endoscopic removal of colorectal adenomas: a randomized clinical trial. Clin Nutr. 2018;37(2):452–8.
[15] Gan R-Y, Li H-B, Sui Z-Q, Corke H. Absorption, metabolism, anticancer effect and molecular targets of epigallocatechin gallate (EGCG): an updated review. Crit Rev Food Sci Nutr. 2018;58(6):924–41.
[16] Siddiqui IA, Adhami VM, Bharali DJ, Hafeez BB, Asim M, Khwaja SI, et al. Introducing nanochemoprevention as a novel approach for cancer control: proof of principle with green tea polyphenol epigallocatechin-3-gallate. Cancer Res. 2009;69(5):1712–6.
[17] Kim B, Park J-E, Im E, Cho Y, Lee J, Lee H-J, et al. Recent advances in nanotechnology with nano-phytochemicals: molecular mechanisms and clinical implications in cancer progression. Int J Mol Sci. 2021;22(7):3571.
[18] Chen B-H, Hsieh C-H, Tsai S-Y, Wang C-Y, Wang C-C. Anticancer effects of epigallocatechin-3-gallate nanoemulsion on lung cancer cells through the activation of AMP-activated protein kinase signaling pathway. Sci Rep. 2020;10(1):5163.
[19] Cai Z-Y, Li X-M, Liang J-P, Xiang L-P, Wang K-R, Shi Y-L, et al. Bioavailability of tea catechins and its improvement. Molecules. 2018;23(9):2346.
[20] Li K, Teng C, Min Q. Advanced nanovehicles-enabled delivery systems of epigallocatechin gallate for cancer therapy. Front Chem. 2020;8:573297.
[21] Mitchell MJ, Billingsley MM, Haley RM, Wechsler ME, Peppas NA, Langer R. Engineering precision nanoparticles for drug delivery. Nat Rev Drug Discov. 2021;20(2):101–24.
[22] Gagliardi A, Giuliano E, Venkateswararao E, Fresta M, Bulotta S, Awasthi V, et al. Biodegradable polymeric nanoparticles for drug delivery to solid tumors. Front Pharmacol. 2021;12:601626.
[23] Siddiqui IA, Adhami VM, Christopher J, Chamcheu, Mukhtar H. Impact of nanotechnology in cancer: emphasis on nanochemoprevention. Int J Nanomedicine. 2012;7:591–605.
[24] Siddiqui IA, Mukhtar H. Nanochemoprevention by bioactive food components: a perspective. Pharm Res. 2010;27(6):1054–60.
[25] Leonarduzzi G, Testa G, Sottero B, Gamba P, Poli G. Design and development of nanovehicle-based delivery systems for preventive or therapeutic supplementation with flavonoids. Curr Med Chem. 2010;17(1):74–95.
[26] Sanna V, Pintus G, Roggio AM, Punzoni S, Posadino AM, Arca A, et al. Targeted biocompatible nanoparticles for the delivery of (−)-epigallocatechin 3-gallate to prostate cancer cells. J Med Chem. 2011;54(5):1321–32.
[27] Sanna V, Singh CK, Jashari R, Adhami VM, Chamcheu JC, Rady I, et al. Targeted nanoparticles encapsulating (−)-epigallocatechin-3-gallate for prostate cancer prevention and therapy. Sci Rep. 2017;7(1):41573.
[28] Necela BM, Crozier JA, Andorfer CA, Lewis-Tuffin L, Kachergus JM, Geiger XJ, et al. Folate receptor-α (FOLR1) expression and function in triple negative tumors. PLoS One. 2015;10(3):e0122209.
[29] Shen J, Hu Y, Putt KS, Singhal S, Han H, Visscher DW, et al. Assessment of folate receptor alpha and beta expression in selection of lung and pancreatic cancer patients for receptor targeted therapies. Oncotarget. 2018;9(4):4485–95.
[30] Ghosh A, Wang X, Klein E, Heston WDW. Novel role of prostate-specific membrane antigen in suppressing prostate cancer invasiveness. Cancer Res. 2005;65(3):727–31.
[31] Kapałczyńska M, Kolenda T, Przybyła W, Zajączkowska M, Teresiak A, Filas V, et al. 2D and 3D cell cultures – a comparison of different types of cancer cell cultures. Arch Med Sci. 2018;14(4):910–9.
[32] Chen C, Ke J, Zhou XE, Yi W, Brunzelle JS, Li J, et al. Structural basis for molecular recognition of folic acid by folate receptors. Nature. 2013;500(7463):486–9.
[33] Boraei ATA, Singh PK, Sechi M, Satta S. Discovery of novel functionalized 1,2,4-triazoles as PARP-1 inhibitors in breast cancer: design, synthesis and antitumor activity evaluation. Eur J Med Chem. 2019;182:111621.
[34] Pala N, Stevaert A, Dallocchio R, Dessì A, Rogolino D, Carcelli M, et al. Virtual screening and biological validation of novel influenza virus PA endonuclease inhibitors. ACS Med Chem Lett. 2015;6(8):866–71.
[35] Morris GM, Huey R, Lindstrom W, Sanner MF, Belew RK, Goodsell DS, et al. AutoDock4 and AutoDockTools4: Automated docking with selective receptor flexibility. J Comput Chem. 2009;30(16):2785–91.
[36] Gasteiger J, Marsili M. Iterative partial equalization of orbital electronegativity – a rapid access to atomic charges. Tetrahedron. 1980;36(22):3219–28.
[37] Morris GM, Goodsell DS, Halliday RS, Huey R, Hart WE, Belew RK, et al. Automated docking using a Lamarckian genetic algorithm and an empirical binding free energy function. J Comput Chem. 1998;19(14):1639–62.
[38] Sanna V, Nurra S, Pala N, Marceddu S, Pathania D, Neamati N, et al. Targeted nanoparticles for the delivery of novel bioactive molecules to pancreatic cancer cells. J Med Chem. 2016;59(11):5209–20.
[39] El-Hammadi MM, Delgado ÁV, Melguizo C, Prados JC, Arias JL. Folic acid-decorated and PEGylated PLGA nanoparticles for improving the antitumour activity of 5-fluorouracil. Int J Pharm. 2017;516(1–2):61–70.
[40] Sanna V, Lubinu G, Madau P, Pala N, Nurra S, Mariani A, et al. Polymeric nanoparticles encapsulating white tea extract for nutraceutical application. J Agric Food Chem. 2015;63(7):2026–32.
[41] Mittal S, Sharma PK, Tiwari R, Rayavarapu RG, Shankar J, Chauhan LKS, et al. Impaired lysosomal activity mediated autophagic flux disruption by graphite carbon nanofibers induce apoptosis in human lung epithelial cells through oxidative stress and energetic impairment. Part Fibre Toxicol. 2017;14(1):15.
[42] Jiang Y, Jiang Z, Ma L, Huang Q. Advances in nanodelivery of green tea catechins to enhance the anticancer activity. Molecules. 2021;26(11):3301.
[43] Zhang G, Zhang J. Enhanced oral bioavailability of EGCG using pH-sensitive polymeric nanoparticles: characterization and *in vivo* investigation on nephrotic syndrome rats. Drug Des Devel Ther. 2018;12:2509–18.
[44] Chavva SR, Deshmukh SK, Kanchanapally R, Tyagi N, Coym JW, Singh AP, et al. Epigallocatechin gallate-gold nanoparticles exhibit superior antitumor activity compared to conventional

gold nanoparticles: potential synergistic interactions. Nanomaterials (Basel). 2019;9(3):396.
[45] Dai W, Ruan C, Zhang Y, Wang J, Han J, Shao Z, et al. Bioavailability enhancement of EGCG by structural modification and nano-delivery: a review. J Funct Foods. 2020;65:103732.
[46] Chan KY, Zhang L, Zuo Z. Intestinal efflux transport kinetics of green tea catechins in Caco-2 monolayer model. J Pharm Pharmacol. 2007;59(3):395–400.
[47] Łukasiewicz S, Mikołajczyk A, Błasiak E, Fic E, Dziedzicka-Wasylewska M. Polycaprolactone nanoparticles as promising candidates for nanocarriers in novel nanomedicines. Pharmaceutics. 2021;13(2):191.
[48] Cabral H, Miyata K, Osada K, Kataoka K. Block copolymer micelles in nanomedicine applications. Chem Rev. 2018;118(14):6844–92.
[49] Elmowafy EM, Tiboni M, Soliman ME. Biocompatibility, biodegradation and biomedical applications of poly(lactic acid)/poly(lactic-*co*-glycolic acid) micro and nanoparticles. J Pharm Investig. 2019;49(4):347–80.
[50] Abedalwafa M, Wang F, Wang L, Li C. Biodegradable poly-epsilon-caprolactone (PCL) for tissue engineering applications: a review. Rev Adv Mater Sci. 2013;34:123–40.
[51] Bellotti E, Cascone MG, Barbani N, Rossin D, Rastaldo R, Giachino C, et al. Targeting cancer cells overexpressing folate receptors with new terpolymer-based nanocapsules: toward a novel targeted dna delivery system for cancer therapy. Biomedicines. 2021;9(9):1275.
[52] Xia W, Low PS. Folate-targeted therapies for cancer. J Med Chem. 2010;53(19):6811–24.
[53] Din F, Aman W, Ullah I, Qureshi OS, Mustapha O, Shafique S, et al. Effective use of nanocarriers as drug delivery systems for the treatment of selected tumors. Int J Nanomed. 2017;12:7291–309.
[54] Fernández M, Javaid F, Chudasama V. Advances in targeting the folate receptor in the treatment/imaging of cancers. Chem Sci. 2017;9(4):790–810.
[55] Xu Q, Yang CH, Liu Q, Jin XF, Xu XT, Tong JL, et al. Chemopreventive effect of epigallocatechin-3-gallate (EGCG) and folic acid on the N-methyl-N'-nitro-N-nitrosoguanidine (MNNG)-induced gastrointestinal cancer in rat model. J Dig Dis. 2011;12(3):181–7.
[56] Liang J, Cao L, Zhang L, Wan X-C. Preparation, characterization, and in vitro antitumor activity of folate conjugated chitosan coated EGCG nanoparticles. Food Sci Biotechnol. 2014;23(2):569–75.
[57] Luo Y, Zhang B, Cheng W-H, Wang Q. Preparation, characterization and evaluation of selenite-loaded chitosan/TPP nanoparticles with or without zein coating. Carbohydr Polym. 2010;82(3):942–51.
[58] Kazi J, Sen R, Ganguly S, Jha T, Ganguly S, Chatterjee Debnath M. Folate decorated epigallocatechin-3-gallate (EGCG) loaded PLGA nanoparticles; in-vitro and in-vivo targeting efficacy against MDA-MB-231 tumor xenograft. Int J Pharm. 2020;585:119449.
[59] Lazzari G, Couvreur P, Mura S. Multicellular tumor spheroids: a relevant 3D model for the in vitro preclinical investigation of polymer nanomedicines. Polym Chem. 2017;8(34):4947–69.
[60] Lovitt CJ, Shelper TB, Avery VM. Advanced cell culture techniques for cancer drug discovery. Biology (Basel). 2014;3(2):345–67.
[61] Białkowska K, Komorowski P, Bryszewska M, Miłowska K. Spheroids as a type of three-dimensional cell cultures-examples of methods of preparation and the most important application. Int J Mol Sci. 2020;21(17):E6225.
[62] Pinto B, Henriques AC, Silva PMA, Bousbaa H. Three-dimensional spheroids as in vitro preclinical models for cancer research. Pharmaceutics. 2020;12(12):1186.
[63] Sims LB, Huss MK, Frieboes HB, Steinbach-Rankins JM. Distribution of PLGA-modified nanoparticles in 3D cell culture models of hypo-vascularized tumor tissue. J Nanobiotechnology. 2017;15(1):67.
[64] Perez JE, Nagle I, Wilhelm C. Magnetic molding of tumor spheroids: emerging model for cancer screening. Biofabrication. 2021;13(1):015018.
[65] Hung H-I, Klein OJ, Peterson SW, Rokosh SR, Osseiran S, Nowell NH, et al. PLGA nanoparticle encapsulation reduces toxicity while retaining the therapeutic efficacy of EtNBS-PDT in vitro. Sci Rep. 2016;6(1):33234.
[66] Michy T, Massias T, Bernard C, Vanwonterghem L, Henry M, Guidetti M, et al. Verteporfin-loaded lipid nanoparticles improve ovarian cancer photodynamic therapy in vitro and *in vivo*. Cancers (Basel). 2019;11(11):E1760.
[67] Chen H, Wei X, Chen H, Wei H, Wang Y, Nan W, et al. The study of establishment of an *in vivo* tumor model by three-dimensional cells culture systems methods and evaluation of antitumor effect of biotin-conjugated pullulan acetate nanoparticles. Artif Cells Nanomed Biotechnol. 2019;47(1):123–31.
[68] Wang X, Zhen X, Wang J, Zhang J, Wu W, Jiang X. Doxorubicin delivery to 3D multicellular spheroids and tumors based on boronic acid-rich chitosan nanoparticles. Biomaterials. 2013;34(19):4667–79.
[69] Ivanova D, Zhelev Z, Aoki I, Bakalova R, Higashi T. Overproduction of reactive oxygen species – obligatory or not for induction of apoptosis by anticancer drugs. Chin J Cancer Res. 2016;28(4):383–96.
[70] Lin S, Fujii M, Hou D-X. Rhein induces apoptosis in HL-60 cells via reactive oxygen species-independent mitochondrial death pathway. Arch Biochem Biophys. 2003;418(2):99–107.
[71] Hou D-X, Uto T, Tong X, Takeshita T, Tanigawa S, Imamura I, et al. Involvement of reactive oxygen species-independent mitochondrial pathway in gossypol-induced apoptosis. Arch Biochem Biophys. 2004;428(2):179–87.
[72] Porporato PE, Filigheddu N, Pedro JMB-S, Kroemer G, Galluzzi L. Mitochondrial metabolism and cancer. Cell Res. 2018;28(3):265–80.
[73] Ma Y-Y, Chen H-W, Tzeng C-R. Low oxygen tension increases mitochondrial membrane potential and enhances expression of antioxidant genes and implantation protein of mouse blastocyst cultured in vitro. J Ovarian Res. 2017;10(1):47.
[74] Jamali T, Kavoosi G, Safavi M, Ardestani SK. In-vitro evaluation of apoptotic effect of OEO and thymol in 2D and 3D cell cultures and the study of their interaction mode with DNA. Sci Rep. 2018;8(1):15787.
[75] Aklima J, Onojima T, Kimura S, Umiuchi K, Shibata T, Kuraoka Y, et al. Effects of matrix pH on spontaneous transient depolarization and reactive oxygen species production in mitochondria. Front Cell Dev Biol. 2021;9:1582.
[76] Vyssokikh MY, Holtze S, Averina OA, Lyamzaev KG, Panteleeva AA, Marey MV, et al. Mild depolarization of the inner mitochondrial membrane is a crucial component of an anti-aging program. PNAS. 2020;117(12):6491–501.